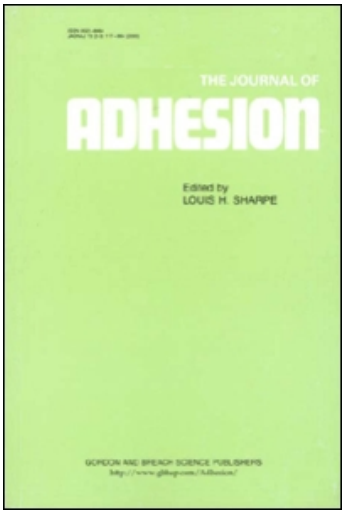

The Journal of Adhesion

Publication details, including instructions for authors and subscription information:
http://www.informaworld.com/smpp/title~content=t713453635

Controlling Interfacial Interpenetration and Fracture Properties of Polyimide/Epoxy Interfaces

Charan Gurumurthy[a]; Edward J. Kramer[b]; Chung-Yuen Hui[c]
[a] Department of Materials, University of California at Santa Barbara, Santa Barbara, California, USA [b] Department of Materials, Department of Chemical Engineering, University of California at Santa Barbara, Santa Barbara, California, USA [c] Department of Theoretical and Applied Mechanics, Cornell University, Ithaca, New York, USA

To cite this Article Gurumurthy, Charan , Kramer, Edward J. and Hui, Chung-Yuen(2006) 'Controlling Interfacial Interpenetration and Fracture Properties of Polyimide/Epoxy Interfaces', The Journal of Adhesion, 82: 3, 239 — 266
To link to this Article: DOI: 10.1080/00218460600646537
URL: http://dx.doi.org/10.1080/00218460600646537

The Journal of Adhesion, 82:239–266, 2006

ISSN: 0021-8464 print/1545-5823 online
DOI: 10.1080/00218460600646537

Taylor & Francis
Taylor & Francis Group

Controlling Interfacial Interpenetration and Fracture Properties of Polyimide/Epoxy Interfaces

Charan Gurumurthy
Department of Materials, University of California at Santa Barbara, Santa Barbara, California, USA

Edward J. Kramer
Department of Materials, Department of Chemical Engineering, University of California at Santa Barbara, Santa Barbara, California, USA

Chung-Yuen Hui
Department of Theoretical and Applied Mechanics, Cornell University, Ithaca, New York, USA

The integrity of an interface between a polyimide and an epoxy is important for a number of microelectronic applications. Here we investigate a surface-modification procedure for the polyimide designed to strengthen its interface with a silica-filled epoxy. The polyimide is chemically modified so that a thin surface layer is converted back to its polyamic acid (PAA) precursor. The modified polyimide is then coated with a solution of the epoxy before dispensing the normal silica-filled epoxy. Interpenetration of the epoxy into the solvent-swollen PAA layer enhances the entanglements between the polymer chains and/or increases the number of primary covalent bonds across the final interface. Increasing the thickness of the PAA layer [measured by Rutherford back scattering spectrometry (RBS)] leads to an increased interpenetration w [measured by secondary ion mass spectrometry (SIMS)]. The fracture energy (G_c^*) of the unmodified polyimide/silica-filled epoxy interface ($w = 12\,nm$) is very low ($\sim 25\,J/m^2$), but G_c^* increases with w until $w = 44\,nm$ ($G_c^* \approx 100\,J/m^2$). Increasing w further leads to an interface that is tougher than the epoxy. The interface can also fail subcritically because of stress-assisted attack of water in the environment (SAWA) on the primary covalent bonds across the interface. We find that increasing w from 12 nm to 38 nm improves the resistance of the interface to SAWA, with the threshold energy release rate (G_{th}^*) for

Received 17 October 2005; in final form 12 January 2006.
One of a collection of papers honoring Hugh R. Brown, the February 2006 recipient of the Adhesion Society Adward for Excellence in Adhesion Science, Sponsored by 3M.

Address correspondence to Edward J. Kramer, University of California Santa Barbara, Department of Materials, Engineering II, 1361C, Santa Barbara, CA 93106, USA. E-mail: edkramer@mrl.ucsb.edu

SAWA increasing by more than sixfold and the steady-state water transport controlled subcritical crack growth velocity (v^*) well above G^*_{th}, decreasing by nearly two orders of magnitude. SIMS is used to probe the fracture surfaces to determine the locus of the crack growth in both our fracture energy samples and our subcritical crack growth samples. In both cases, the interface with an unmodified polyimide surface fails along the interface, and the modified interfaces ($12\,nm < w < 44\,nm$) typically fail within the newly created interpenetrating epoxy/polyimide interphase.

Keywords: Epoxy; Fracture energy; Interface; Poly(amic acid); Polyimide; Rutherford backscattering spectrometry; Secondary ion mass spectrometry

INTRODUCTION

Hugh Brown's many fundamental contributions to adhesion science should not overshadow the fact that he applied these concepts to important technological adhesion problems, in particular the adhesion of polyimide to polyimide. He showed in particular that the state of cure of a polyimide substrate was very important in its adhesion to a subsequent layer of polyimide formed by spinning on the same polyimide precursor and curing the entire bilayer [1]. He demonstrated that diffusive interpeneration was crucially important in the development of adhesion for such systems. Exploiting these ideas, we have investigated the strengthening of an interface between a polyimide and an epoxy. This interface is important in many microelectronic applications. A salient example is a direct chip attach (DCA) microelectronic assembly [2] shown schematically in Figure 1. DCA technology involves mounting an unpackaged silicon die directly onto a printed circuit board (PCB) using solder joints as mechanical and electrical links between the DCA and the PCB. A 1–5-μm thick polyimide (referred to as passivation) protects the active side of the component. The polyimide is in direct contact with the silica-filled epoxy (referred to as underfill) that encapsulates the solder joints, thereby increasing its reliability [3,4].

In DCA and many other applications, epoxy should adhere well to the polyimide [5] possessing both high fracture energy and good resistance to subcritical crack growth under thermal and hydrothermal conditions. However, because of its closed ring structure, polyimide adheres poorly to the epoxy, leading to poor fracture energy [6] and poor subcritical crack-growth resistance under thermal [7] and or hydrothermal [6] conditions. A recent review of previous work on such interfaces, as well as a set of measurements of the fracture energy of

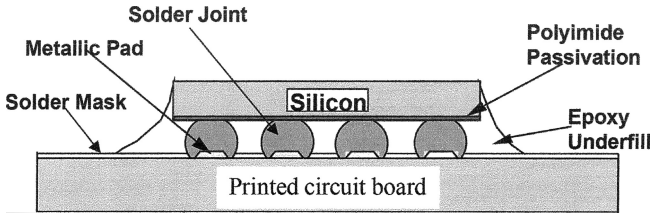

FIGURE 1 Schematic of a direct chip attach (DCA) microelectronic assembly. The weakest link in this system is the interface between the underfill (silica-filled epoxy) and the polyimide passivation.

unmodified interfaces between four different polyimides and a bisphenol-F epoxy, have been given by Hoontrakul *et al*. [8]. Strengthening this interface has numerous potential benefits. Many techniques have been tried to strengthen the polyimide interface with metals and other polymers. These primarily include ion-beam and plasma treatments of the polyimide surface [9–13]. These treatments roughen the polyimide surface, causing mechanical interlocking at the interface, and alter the chemical structure of the polyimide surface, thus potentially enabling covalent chemical bonding across the interface. Verifying that such chemical bonds actually form and strengthen the interface is nearly impossible.

In this work we exploit a different method of modifying the polyimide surface using an aqueous base treatment that was first developed by Lee and coworkers at IBM [14–19] and recently used to strengthen polyimide/epoxy interfaces by Kim *et al*. [20]. A superficially similar method for strengthening polyimide interfaces with epoxy by treating the polyimide surface with diamines was developed by Yun *et al*. [21]. This method produces a surface layer in which the polyimide is converted back into its polyamic acid (PAA) precursor. The thickness of the PAA layer can be accurately controlled. The PAA layer can then be penetrated by the epoxy, thus leading to entanglement [22–24] and perhaps covalent bonding with the epoxy after a final curing step. Rutherford backscattering spectrometry (RBS) has been used to measure the thickness of the PAA layer, and secondary ion mass spectrometry (SIMS) has been used to measure the interpenetration of the epoxy into the PAA layer.

We have used an asymmetric double-cantilever beam technique (ADCB) to measure the fracture energy (per unit area), G_c^*, of the modified interface. The fracture energy increases linearly with interpenetration distance, w, until the interface is so strong that the crack

propagates through the bulk epoxy. The water-assisted subcritical crack-growth velocity (v) at various values of G^*, the strain energy released per unit area crack advance, commonly called the strain-energy release rate, was also measured using an ADCB setup, modified to allow us to control the temperature (T) and relative humidity (RH) of the environment. A model developed previously [25] is used to fit the measured data. The surface-modification procedure increases the threshold strain-energy release rate (G^*_{th}) for subcritical crack growth. The larger the interpenetration, w, the lower the v is for a given $G^* > G^*_{th}$.

MATERIALS

DGEBA (diglycidyl ether of bisphenol-A) was obtained from Dow Chemical Co, Freeport, TX (DER 331). TETA (triethylene tetramine), obtained from Aldrich, Milwaukee, WI, was used as the hardener to crosslink the DGEBA. PI 2545 PMDA/ODA polyimide precursor (Dupont, Wilmington, DE) was used as the precursor for the polyimide. The epoxy used was a 3,4 epoxy cyclohexyl methyl-3,4 epoxy cyclohexyl carboxylate (ERL 4221, obtained from Union Carbide (now Dow Chemical Co., Midland, MI). Hexahydro-4-methylphthalic anhydride (obtained from Aldrich, Milwaukee, WI) was used as a hardener to cure the epoxy. A catalyst (N-N dimethyl benzyl amine) (Aldrich, Milwaukee, WI) and an initiator (ethylene glycol) (Aldrich, Milwaukee, WI) were added to accelerate the curing mechanism of the epoxy system [25]. The epoxy is prepared by 1:1 ratio by weight of the epoxy and the anhydride and 5% by weight each of the catalyst and the initiator [25]. Fused silica particles used as filler were obtained from the Inabata Corporation, Toyko, Japan. The addition of the silica filler particles to the epoxy system has been detailed before [25]. Tetramethyl ammonium hydroxide (TMAH), glacial acetic acid (CH_3COOH), cesium nitrate ($CsNO_3$), and dimethyl sulfoxide (DMSO) were obtained from Aldrich, Milwaukee, WI.

SAMPLE PREPARATION

Major portions of our sample preparation procedure have been reported before [25]. Hence, only a brief sketch is provided here with a detailed description of the surface-modification procedure. DGEBA epoxy resin was melted, and TETA was added to the resin. An excess molar ratio of the amine hydrogens to the epoxy group is provided to improve the adhesion of the polyimide with the DGEBA epoxy plate. (This interface is strengthened to avoid crack propagation along the

wrong interface.) The molten epoxy was then allowed to flow into a glass sandwich mold using a frame cut from a Teflon® sheet as a spacer [26]. The surface of the glass mold was precoated with a self-assembled monolayer of octadecyltrichlorosilane (OTS) to prevent the epoxy from adhering to the glass plate [27].

The epoxy slab (80 mm × 50 mm) was partially crosslinked in the mold. It was removed from the mold and then spin-coated with a thin layer (3–5 microns) of PMDA/ODA precursor. The polyimide precursor was imidized in air at 265°C for 2 h. During the imidization process, the polyimide precursor reacts with the extra amine functional groups on the DGEBA epoxy plate to form strong chemical bonds at the interface. Because of the thermal expansion mismatch between the polyimide and the DGEBA, the plate warped when cooled from the cure temperature to the room temperature. Hence, after imidization, the polyimide-coated plate was clamped between two OTS-coated glass plates and annealed for another 20 min at 265°C. The mold was then cooled down while the plate is still held firmly by the glass plates.

A schematic of the surface modification procedure [14–19] for the polyimide is presented.

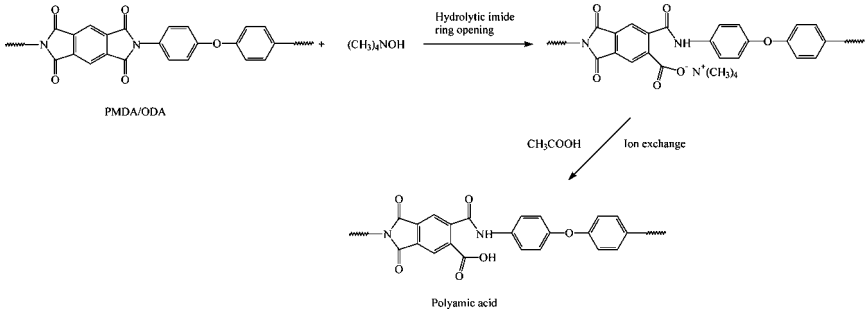

The polyimide side of the DGEBA plate is soaked in a 1 M solution of TMAH at room temperature for various lengths of time. The polyimide rings are opened by the basic solution, leading to the formation of an ammonium salt [14–19], in a layer whose thickness increases linearly with soaking time.

We then conduct an ion-exchange by soaking the modified polyimide surface layer in a 1 M acetic acid for 10 min at room temperature. This enables us to convert the modified surface of the polyimide back into its precursor polyamic acid.

We then clad the surface-modified polyimide with an epoxy film (∼1.5 μm thick) spun cast from solution in DMSO. DMSO was selected for two primary reasons: (a) it is a good swelling agent for the polyamic

acid and (b) it does not contain nitrogen in its chemical structure. The latter is an advantage, because, as explained in the next section, DMSO does not affect the CN^- (carbon–nitrogen negative ion) SIMS signal used to identify the interface. The solvent swells the PAA layer and enhances the interpenetration [28] of the epoxy chains into the polyamic acid layer.

The epoxy-clad, surface-modified, polyimide-coated DGEBA plate is again placed between two OTS-coated glass plates with a Teflon® spacer, and the silica-filled epoxy is flowed atop the spun-cast epoxy. The epoxy system is left at room temperature for ~12 h to gel. It is then cured by the following step-cure process: the mold is ramped from room temperature to 90°C at the rate of 4°C per min and held at 90°C for 1 h. This thermal pretreatment is followed by ramping the temperature from 90°C to 150°C at the rate of 4°C per min. The curing is then

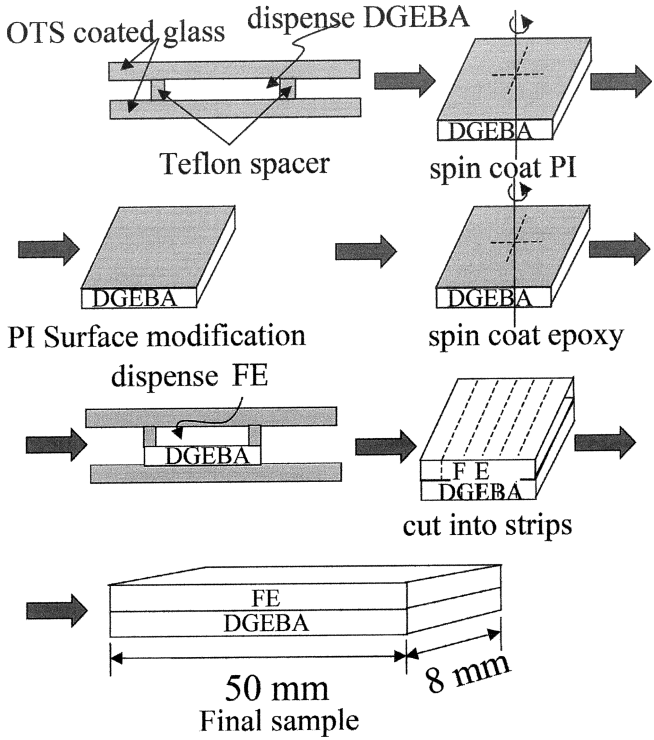

FIGURE 2 Schematic of the sample preparation procedure. Here, OTS stands for octadecyl trichlorosilane, DGEBA stands for diglycydyl ether of bisphenol-A, PI stands for polyimide (PMDA/ODA precursor), FE stands for filled model epoxy.

finished by holding the sample at 150°C for 3 h. The step-cure procedure is followed so that bubble formation due to out-gassing is avoided by initiating the cross-linking at the lowest possible temperature [25]. The sample is then cooled within the mold to avoid warpage due to the thermal mismatch between the filled epoxy and the DGEBA plate. A thermocouple is used to monitor the temperature of the mold during the cooling process, and the mold is removed at the desired temperature for the fracture tests. The samples thus obtained are cut with a diamond saw into strips that are 50 mm long and 8 mm wide. The sample preparation procedure is presented schematically in Figure 2.

RESULTS AND DISCUSSION

Hydrolysis and Interpenetration Depth

The depth to which the ring opening has taken place because of the chemical surface modification procedure of the polyimide is determined as follows: we coat a commercial adhesion promoter (DuPout VM 651, DuPont, Wilmington, DE) onto the surface of a silicon wafer. The adhesion promoter is step-baked at 60°C for 20 min and 80°C for 20 min. The polyimide precursor is then spin cast on the surface of the adhesion promoter and cured. The cured thickness of the polyimide film is $\sim$3.5 μm. We carry out the surface modification procedure just as mentioned in the previous section. The surface-modified polyimide is then soaked in 1 M cesium nitrate ($CsNO_3$) at room temperature for 24 h. An ion-exchange (Cs^+ for H^+) process occurs in which the –COOH groups of the PAA are converted into their Cs^+ salt. We then conduct RBS to depth profile cesium.

In RBS, monoenergetic helium ions (α particles) incident on the sample undergo elastic collision with the nuclei in the sample and are scattered backward into an energy-sensitive detector. The detector measures the energy of the backscattered He^{++} ions, which quantifies the mass of the target nucleus from which the incident particle was scattered. The yield, which is the number of backscattered He^{++}/per incident ion, is proportional to the target atom concentration. He^{++} ions that are scattered from the target nuclei that are present beneath the surface arrive at the detector with reduced energies, with the decrease in energy proportional to the depth. The raw spectra consist of ion yield *versus* energy. A simulation procedure (RUMP^{TM}) is then used to convert the energy to hydrolysis depth and the ion yield into the concentration of cesium. These spectra show that all the imide rings are opened in a surface layer whose thickness increases linearly

with time. Our results are consistent with previous experiments [29] and are shown in Figure 3, where it can be seen that the ring-opened layer (PAA) thickness increases at the rate of 2.5 nm/min under our conditions (1 M TMAH at room temperature). The rate at which the PAA thickness increases can be increased by increasing either the temperature of the basic solution or the molarity of the TMAH [29,30]. At long times at higher temperatures or TMAH molarity, however, hydrolysis of the main chain amide bond of PAA and subsequent etching of the surface occurs. Under the conditions used in these experiments, no etching occurs.

The depth to which the epoxy chains interpenetrate the PAA surface layer is determined as follows: polyimide films on a silicon substrate whose surfaces had been modified to various depths were spin coated with an epoxy ($\sim$1.5 μm thick). The epoxy is cured according to the schedule. Dynamic secondary ion mass spectrometry (SIMS) is used to determine the composition ratio of the various chemical species as a function of depth. A brief description of the SIMS technique is provided.

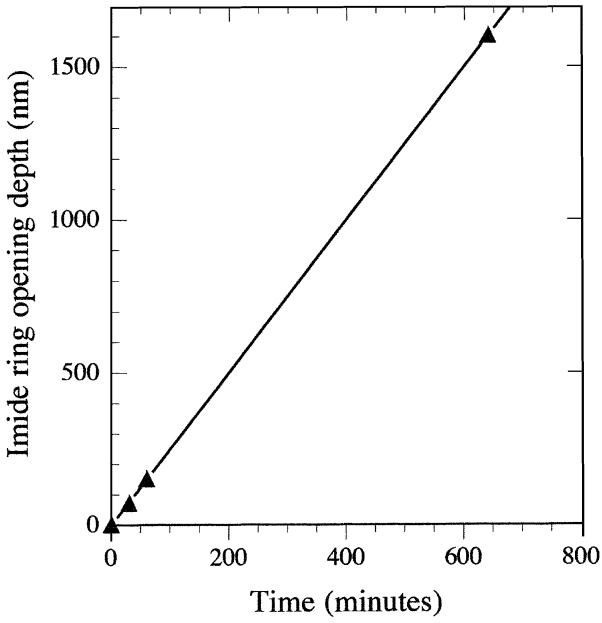

FIGURE 3 Imide ring-opening depth (in nm) as measured by RBS due to exposure of the polyimide to TMAH at room temperature for various time intervals (in min).

We use a rastered oxygen ion (O_2^+) primary beam to sputter away the surface of the sample forming a flat-bottomed crater $300\,\mu m \times 300\,\mu m$. The sputtered species contain elements as neutrals in various excited states, ions with one or more positive or negative charges and clusters of the particles. The sputtered negative ions are extracted from the central region of the crater (less than one tenth of the total area) and are analyzed by a quadrapole mass analyzer. The relative abundance of the sputtered ions provides a direct measure of the composition of the layer that has been removed. As sputtering proceeds, a depth profile of the elements of interest is obtained. SIMS requires a certain sputtering depth, typically 10 nm, before steady state is reached. This transient is due to the time required for a steady-state ion damage profile to build up on the surface of the sample. Beyond this steady-state depth, the relative abundance of the ions truly corresponds to the composition ratio in the sample. There are ways to avoid the initial transient. One way is to coat the surface with a sacrificial layer. In our experiments, for all samples from which the information from the surface is desired, we have floated an $\sim 0.1\,\mu m$ polystyrene (PS) sacrificial layer onto the sample surface. The raw profile obtained from SIMS contains secondary ion counts per unit time (on the Y-axis) as a function of sputtering time (on the X-axis). The sputtering time can be converted to sputtering depth by determining the crater depth using a scanning force microscope (SFM) or a mechanical profilometer. The Y-axis can be converted into absolute concentration by comparing the composition ratio obtained from SIMS with that obtained from an absolute characterization technique such as RBS or forward recoil spectrometry (FRES). In our experiments, we have not converted the Y-axis to concentration but we have converted the sputter time (on the X-axis) to sputter depth.

We can identify the interface between the epoxy and the polyimide based on the CN^- signal. The epoxy generates very little CN^- signal, which comes from the nitrogen present in the catalyst used in curing this system. However, there is a very strong CN^- signal from the high concentration of nitrogen in the polyimide. Figure 4a shows the CN^- depth profile of the epoxy cured on the polyimide when there is no surface modification of the polyimide. Figure 4b shows the CN^- depth profile of the epoxy cured on the polyimide that has been converted to PAA to a depth of ~ 1600 nm (as determined through RBS). The resolution of SIMS under our operating conditions is ~ 12 nm. Hence, we conclude that there is very little interpenetration of the epoxy into the polyimide when the polyimide has not been modified. We have also verified that the interface between a surface-modified polyimide (imide ring opened to a depth of ~ 50 nm) and the epoxy dispensed without the solvent is sharp (~ 16 nm); *i.e.*, the presence of the solvent

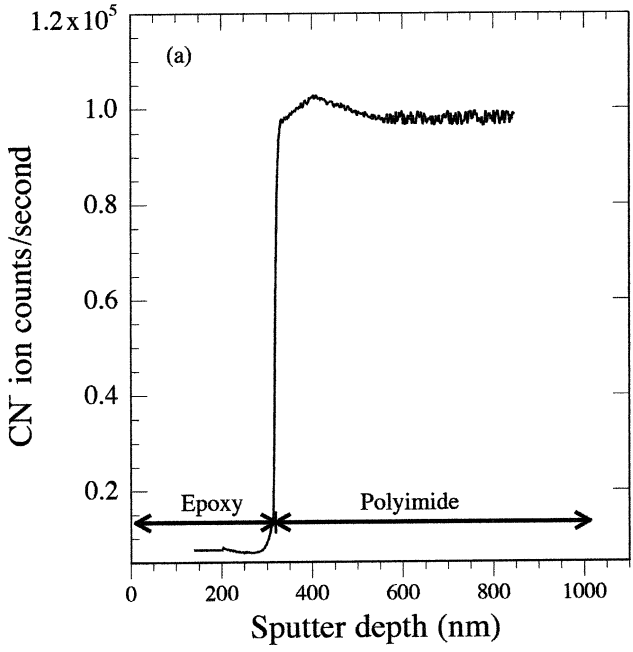

FIGURE 4 SIMS depth profiles obtained for a polyimide/epoxy interface produced from (a) an untreated PI surface and (b) a PI surface treated for 640 min in TMAH at room temperature, respectively. When the PI surface is left untreated, the width of the interface is $\sim$12 nm, very close to the depth resolution of the SIMS technique. The width of the interface when the polyimide has been surface treated for 640 min (and shown by RBS to have been converted to PAA to a depth of $\sim$1600 nm) is much larger: $\sim$700 nm.

is essential for the interpenetration of the epoxy chains into the PAA layer. However, once the polyimide surface has been converted to PAA, the interpenetration of the epoxy (in the presence of solvent) into the polyimide is substantial as seen in Figure 4b. Figure 5 shows that the epoxy interpenetration depth increases as a function of time of exposure of the polyimide to the 1 M TMAH solution. The epoxy interpenetration due to the swelling of the modified polyimide layer by the solvent (as measured by SIMS) increases linearly with time at the rate of $\sim$1 nm/min of exposure to TMAH solution at room temperature.

Figure 6 shows the interpenetration depth (as measured by SIMS) as a function of the depth of hydrolysis of the polyimide (as measured by RBS). The inset in Figure 6 presents only that part of our data that is of relevance for the fracture energy and the subcritical crack-growth

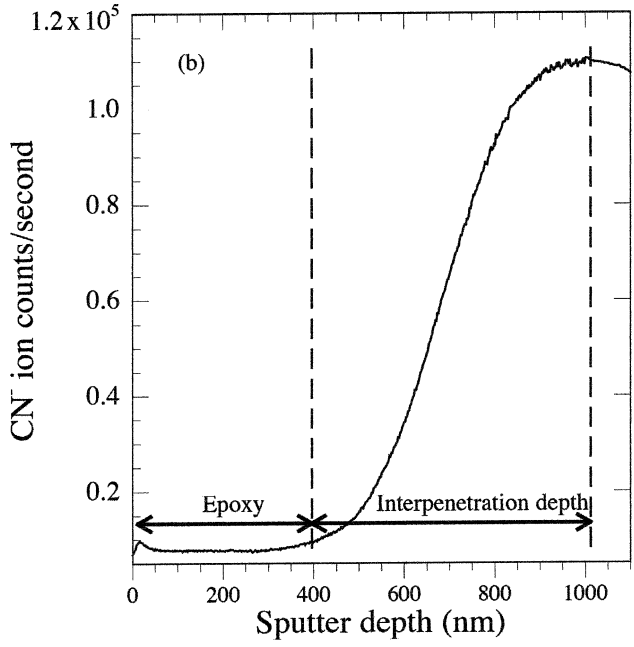

FIGURE 4 Continued.

measurements presented later. As seen from Figure 6, initially, when the hydrolysis depth is very small, the interpenetration depth nearly matches the hydrolysis depth. However, under larger hydrolysis depths, the interpenetration depth lags behind the hydrolysis depth. The major reason for this may be due to the fact that the DMSO solvent used for spin casting the epoxy is also a good solvent for the polyamic acid. Hence, some thickness of the polyamic acid layer could have been washed away during spin casting [18].

The following paragraphs describe the measurement of the fracture energy of the modified interface and the measurement of the steady-state subcritical crack growth velocity along the interface due to water attack.

Fracture Energy

The fracture energy of the polyimide/epoxy interface is determined by using an ADCB technique [31,26]. The detailed procedure has been reported earlier [25]. A 0.3-mm-thick razor blade is driven at a constant rate of 3 μm/s along the interface. The crack length was

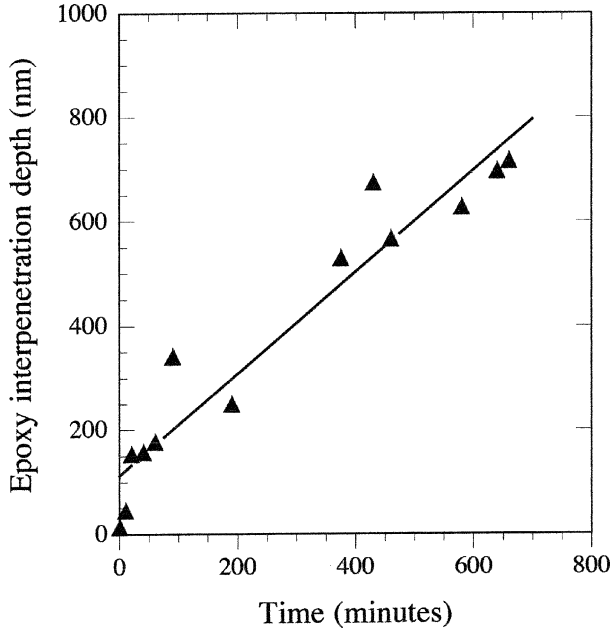

FIGURE 5 Epoxy interpenetration depth into the surface-modified polyimide (in nm) *versus* the time of exposure of the polyimide to TMAH solution at room temperature (in min).

measured at eight different times. Then the original razor blade was replaced by a 0.6-mm-thick blade, and the test was continued. Again eight measurements of the crack length were made. The mechanical energy release rate (G_{mech}) along the interface is a function of the thickness of the razor blade, the dimensions of the specimen, and the elastic properties of the specimen [32]. However, the mismatch in the coefficient of thermal expansion (CTE) between the DGEBA beam and our epoxy leads to an additional strain-energy release rate (G_{r}) at the crack tip due to the thermal residual stresses caused by the CTE mismatch. Hence, we have modified the equations for G_{mech} to include the effect of G_{r}. The modified energy-release rate is referred to as G^*. For a given sample (*i.e.*, fixed geometry and material properties), the crack length a is the only parameter that controls the G^*. When the razor blade is introduced and moved along the interface, the crack tip does not move until the crack length reaches the critical value. Then a steady-state crack growth occurs. We determine the fracture energy G_{c}^* from the critical crack length. All equations necessary for determining G^* can be found in Ref. 26.

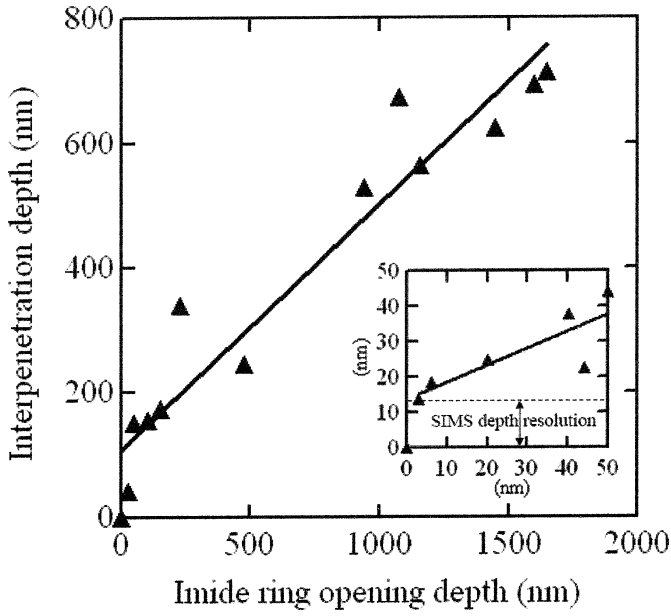

FIGURE 6 Interpenetration depth of the epoxy into polyimide (as measured by SIMS) *versus* depth of the hydrolyzed polyimide layer (measured by RBS). We believe that the interpenetration depth is less than the imide ring-opening depth because of dissolution of some of the polyamic acid in the solvent (DMSO) used for spin casting the epoxy.

In general, G_c^* is sensitive to the mechanical phase angle (ψ). Normally, the phase angle can be varied by varying the ratio of thickness of the silica-filled epoxy to that of the DGEBA beams. However, for the present samples, the thickness ratios between 0.52 ($\psi = 20.6^\circ$) and 2.0 ($\psi = 14.3^\circ$) did not change the phase angle significantly [25], and, hence, G_c^* is nearly a constant for these thickness ratios. Hence, all our experiments have been conducted with a constant thickness ratio of 0.52.

Figure 7 shows the fracture energy of the epoxy/polyimide interface measured as a function of the epoxy interpenetration depth, obtained through SIMS. It is seen that even when the interpenetration has reached only $\sim$45 nm, the fracture energy increases fourfold to $\sim 100\,J/m^2$. G_c^* of samples with higher interpenetration ($\sim$110 nm and higher) could not be measured because the interfacial fracture energy became higher than the fracture energy of the individual epoxy beams on either side of the interface, and, hence, they fractured before the interface could fracture.

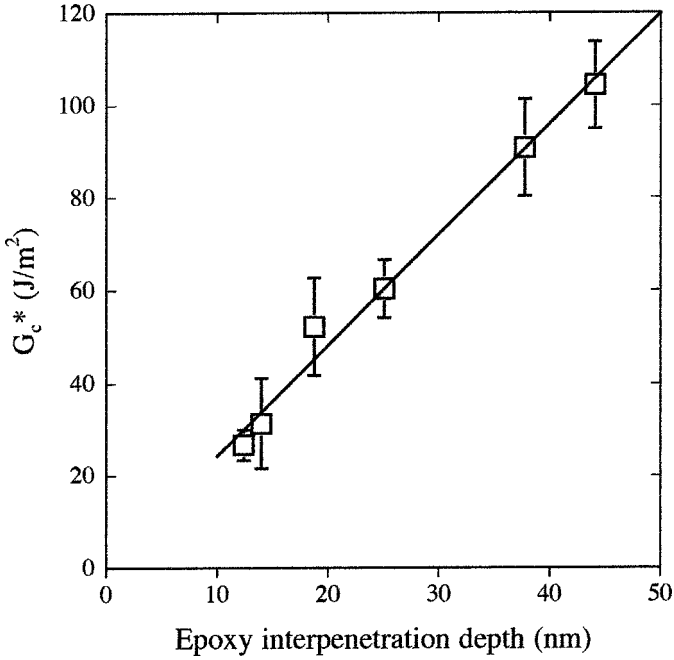

FIGURE 7 Plot of the fracture energy (G_c^*) as a function of the epoxy interpenetration depth into the surface-modified polyimide (measured using SIMS). The solid line shown is a least squares fit to the data.

Our results on the strengthening of the polyimide/epoxy interface as a function of the interpenetration depth of the epoxy into the PAA layer can be compared with previous reports on strengthening the polymide/polyimide interface by the interpenetration technique. It has been shown by peel testing that the fracture energy G_c^* of the polyimide/polyimide interface without any surface modification [1,33] is less than $10\,J/m^2$. The G_c^* remains at that value for w up to $\sim 30\,nm$. However, increasing the w beyond $\sim 30\,nm$ progressively increases the G_c^*. At $w \approx 50\,nm$, the G_c^* is so high that that it cannot be reliably measured by the peel-testing technique. When $w \approx 200\,nm$, the G_c^* of the interface reaches that for the bulk polyimide [1,33]. Lee found a similar adhesion enhancement for a polyimide/polyimide interface as a function of modification depth even after the PAA surface layer was thermally treated to convert the PAA to an amorphous polyimide [34]. Although Kim *et al.* [20] did not measure the depth to which their polyimide layer was converted to PAA by treatment for various

times with 1 M KOH, their results are qualitatively consistent with ours. However, they attribute all strengthening of their interface to reaction between the polyamic acid surface and the epoxy, whereas, as we have shown, a very thin surface layer of polyamic acid is not sufficient to achieve maximum fracture energy. A significant interpenetration of the epoxy into the polyamic acid layer before final cure is necessary to obtain the largest G_c^*.

Locus of Failure in the Fracture Energy Samples

We have determined the locus of the crack propagation in our samples used for measuring the fracture energy using SIMS. After fracture, we float a thin layer of polystyrene (PS) ($\sim$100 nm thick) onto our fracture surfaces. PS acts as our sacrificial layer so that we could get surface information from our fracture surface using SIMS. This is determined using the CN^- signal, as mentioned earlier. When no surface modification was carried out, SIMS results clearly show that the fracture occurs along the weak epoxy/polyimide interface. However, when the interpenetration width increases, we see evidence that both polyimide and epoxy are present on both sides of the fracture surface. Hence, in these cases, the crack propagates through the newly created interpenetrating epoxy/polyimide interphase. Table 1 summarizes the results obtained. These data are severely affected by the loss of resolution of the SIMS technique due to the roughness

TABLE 1 Thickness of the Epoxy on the Polyimide Fracture Surface and Thickness of the Polyimide on the Epoxy Fracture Surface as Measured by SIMS on the Fracture Energy Samples

Interphase width (nm)	Thickness of epoxy on the polyimide side of the fracture surface (nm)	Thickness of polyimide on the epoxy side of the fracture surface (nm)
12 (no modification)	0	0
19	18	14
38	22	33
44	39	46

Notes: The interphase width was measured without fracturing the interface. An interphase width of 12 nm corresponds to the case where no surface modification was performed. All the interphase width measured for that sample is believed to arise from the instrumental resolution of the SIMS technique. The numbers in columns 2 and 3 do not add up to numbers in column 1 because of the degradation of the SIMS resolution caused by the roughness of the fracture surfaces.

of these fracture surfaces. Figure 8 shows the topography of the fracture surfaces obtained using scanning electron microscopy (SEM). It is clear that the fracture surfaces of the unmodified interface are very smooth with no evidence of local plastic deformation. However, the fracture surfaces of an interface with an interpenetration w of 44 nm show evidence of severe plastic deformation. Our results are similar to those obtained for the polyimide/polyimide interface reported earlier [31]. For this interface, the fracture surfaces produced by peel testing when $w < 30$ nm are very smooth, but these become progressively rougher as w increases further. The increased stress transfer due to interpenetration strongly increases the size of the zone of local plastic deformation of the polyimide and thus leads to a rough surface.

Subcritical Crack Growth due to Water Attack

Frequently epoxy/polyimide interfaces are exposed to high temperature and humidity during service or reliability testing. For example, the underfill epoxy/polyimide passivation interface in a DCA microelectronic device typically has to withstand a temperature of about $\sim$80°C and RH of $\sim$85% during real-life operation. The presence of large thermomechanical stresses along the interface, combined with the attack by the environmental water on the stretched covalent bonds across the interface, can lead to stress corrosion, where the interface can fail much below the critical energy-release rate required for breaking bonds under dry conditions. Our detailed measurements of the subcritical crack growth velocity, v, for an unmodified polyimide/filled-epoxy interface at various temperatures (when RH is held constant) and at various RHs (when temperature is held constant) have been reported elsewhere [25]. In this article, we have selected a specific condition ($T = 80$°C and $RH = 100\%$) and measured v for various depths of epoxy interpenetration, w, into the polyimide. The data obtained when there is no polyimide surface modification and when the polyimide surface is modified so that w is 19, 25 and 38 nm, respectively, are shown in Figure 9. As mentioned earlier, the measured w for the unmodified polyimide surface is $\sim$12 nm, which is the resolution of our SIMS technique. Figure 9 clearly shows the decrease in v and the increase in the threshold energy-release rate (G^*_{th}) when w is increased. This effect is believed to be due to the increased entanglement and perhaps chemical bonding across the interface. The solid lines shown in Figure 9 are fits obtained using a model reported earlier [25], which is briefly described in a later section of this article.

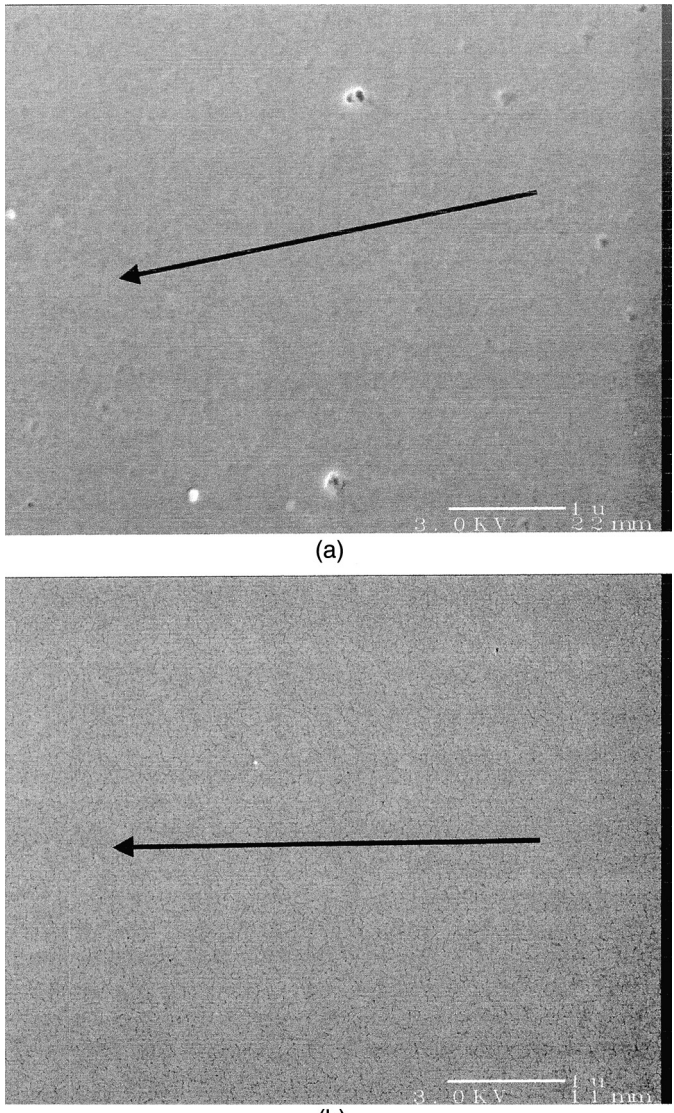

FIGURE 8 Topography of the fracture surfaces of the fracture energy samples: (a) and (b) show the epoxy and the polyimide sides, respectively, of the fractured unmodified polyimide/epoxy interface whereas (c) and (d) show the epoxy and the polyimide sides, respectively, of the fractured sample with $w = 44$ nm. The arrow in the figures represents the direction of the crack propagation.

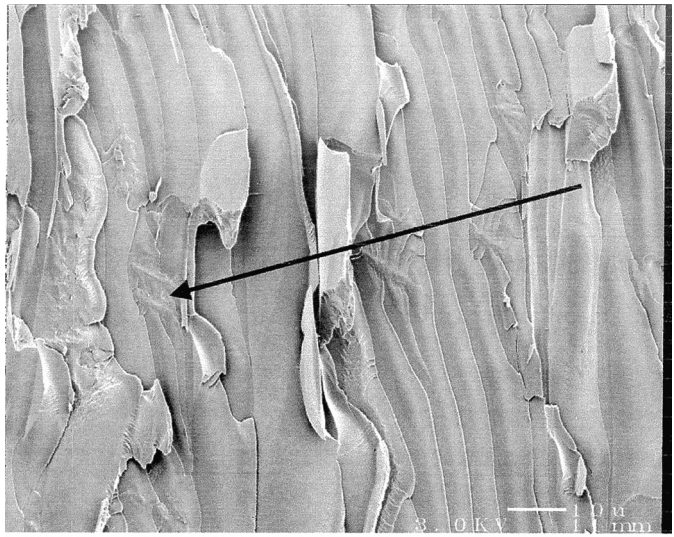

(c)

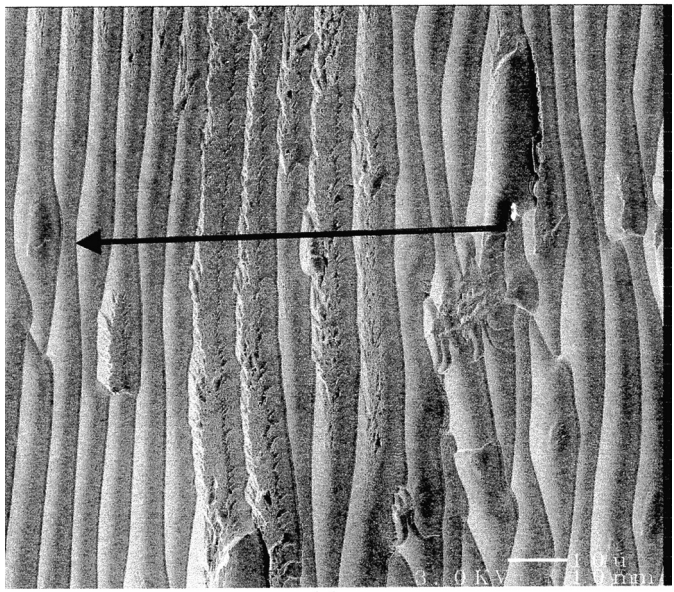

(d)

FIGURE 8 Continued.

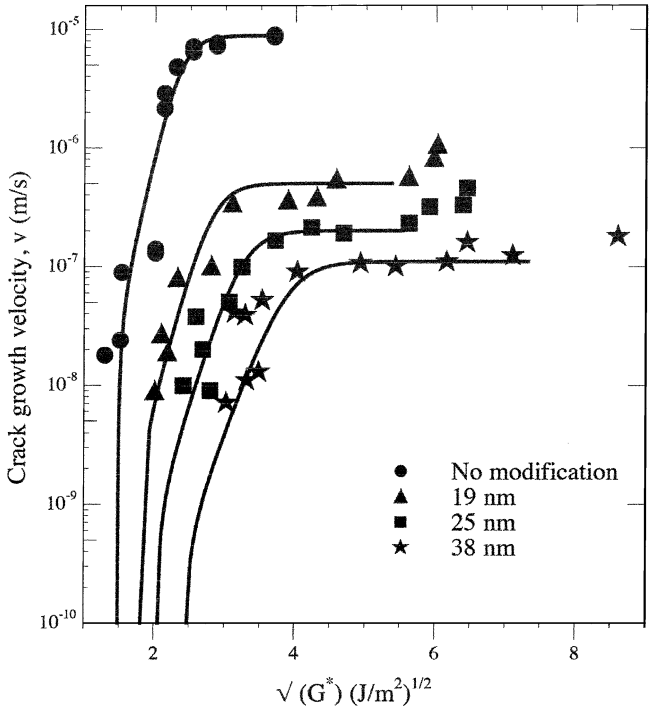

FIGURE 9 Logarithm of the steady-state subcritical crack growth velocity (v) plotted against the square root of the strain energy release rate at the crack tip (G^*). The numbers in the legend represent the depth to which interpenetration of the epoxy into the polyimide has occurred (obtained using SIMS).

Locus of Failure in Subcritical Crack Growth Samples

The location of the failure in our subcritical crack-growth samples can be determined using SIMS after the crack propagates subcritically for a sufficient distance along the interface. Because the subcritical crack-growth measurements were made for many different G^* values along the same interface, the G^* that the sample experienced at the location where the SIMS analysis was conducted is not precisely known. However, because our SIMS results are the same at a variety of locations (*i.e.*, different G^*s) the location of subcritical crack growth does not depend significantly on G^*. As before, PS was used as the sacrificial layer on our fracture surfaces. Figures 10a and 10b show the epoxy side and the polyimide side of the interface after fracture for the unmodified polyimide/epoxy interface. If polyimide is present on the epoxy

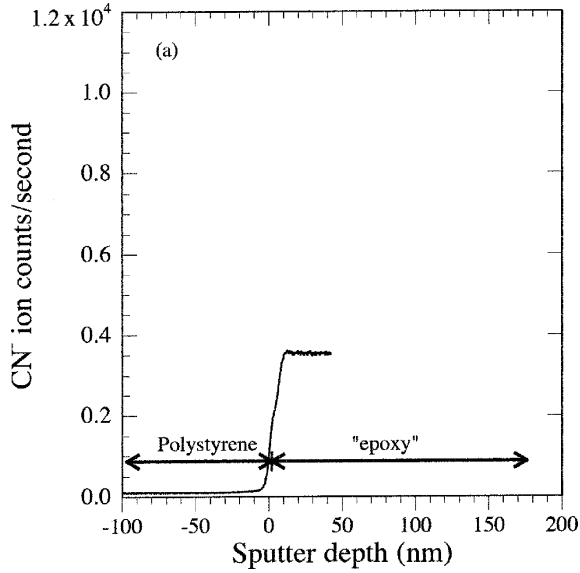

FIGURE 10 SIMS analysis on the fracture surfaces. PS is floated onto the surface of the sample as a sacrificial layer: (a) the epoxy side of the unmodified interface, (b) the PI side of the unmodified interface, (c) the epoxy side of the interface when the PI surface was modified so that the interpenetration of the epoxy into the PI was 25 nm, and (d) the PI side of the interface when the PI was modified as mentioned in (c).

fracture surface then the corresponding CN^- signal will show a surface peak. The very fact that Figure 10a does not exhibit this behavior implies that the subcritical crack growth does not occur into the bulk polyimide. By similar argument, from Figure 10b, it is clear that the subcritical crack growth does not occur through the bulk epoxy (there would be a layer of epoxy on the polyimide side of the interface, and SIMS shows that there is none). Hence, we can conclude that the subcritical crack occurs along the interface between the unmodified polyimide and the epoxy (similar to our results in the unmodified fracture energy samples). Figures 10c and 10d show the SIMS depth profiles obtained from the epoxy and the polyimide sides of the fracture of a sample whose interface was modified so that epoxy interpenetration into the polyimide had occurred to a depth of 25 nm. It is clear from the figure that the crack is propagating along the interpenetration region. Table 2 summarizes the location of crack growth for the various interpenetration depths. We find that the subcritical crack growth in the modified interfaces occurs close to the middle of the newly

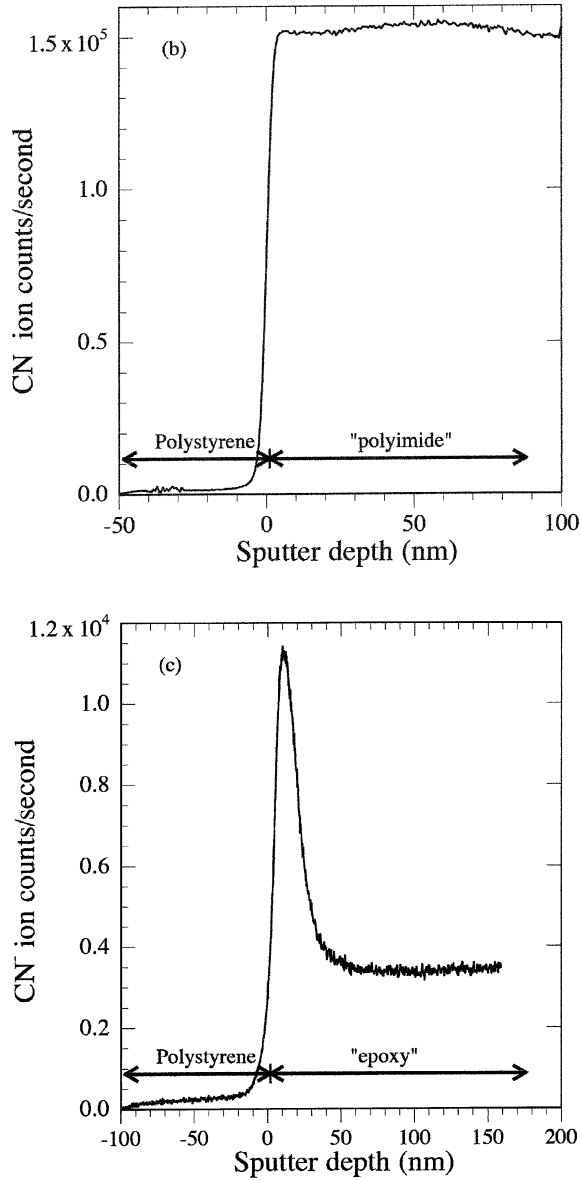

FIGURE 10 Continued.

created interpenetrated epoxy/polyimide interphase. The thickness measurements on either side of the fracture surface add up to numbers that are much closer to the measured w in this case than

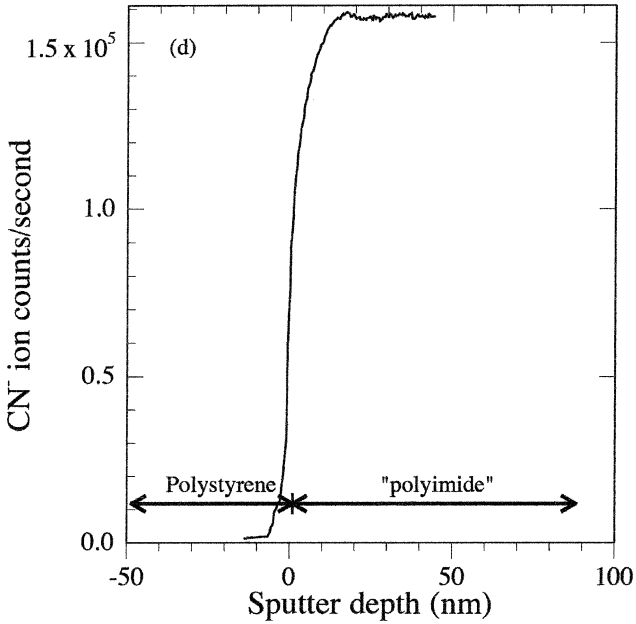

FIGURE 10 Continued.

in the fracture energy samples. This is because the fracture surfaces of the subcritical crack growth samples are much smoother than those of the fracture energy samples (confirmed by SEM).

TABLE 2 Thickness of the Epoxy on the Polyimide Fracture Surface and Thickness of the Polyimide on the Epoxy Fracture Surface as Measured by SIMS on the Subcritical Crack Growth Samples

Interphase width (nm)	Thickness of epoxy on the polyimide side of the fracture surface (nm)	Thickness of polyimide on the epoxy side of the fracture surface (nm)
12 (no modification)	0	0
19	13	11
25	14	17
38	27[a]	21[a]

Notes: The interphase width in column 1 was measured without fracturing the interface. An interphase width of 12 nm corresponds to the case where no surface modification was performed. All the interphase width measured for that sample is believed to arise from the instrumental resolution of the SIMS technique.

[a]Averaged over three measurements at different locations.

Modeling of the Subcritical Crack Growth along the Polyimide/Epoxy Interface

Our model follows along the general lines of a classical model [35] for subcritical cracking of glass by water. The basis of our model is that the subcritical crack growth is the result of the stress-assisted hydrolysis of ester bonds at the crack tip. Our surface-modification procedure can be modeled as increasing the number of ester bonds that are present across the interface, *i.e.*, assuming that entanglement is also equivalent to primary covalent bonds across the interface. This ester hydrolysis reaction can be represented as a thermally activated process [25]. The free energy change associated with the presence of stresses at the crack tip can be represented as $\beta\sqrt{G^*}$, where β is a material constant ($\propto V^*/\sqrt{L}$, where V^* is the activation volume and L is an arbitrary length scale that is of the order of the distance between two successive covalent bonds across the interface) and G^* is the strain-energy release rate at the crack tip.

Our model describes two of the three regimes of subcritical crack growth [25]. When G^* is below a threshold energy rate G^*_{th}, the stress at the crack tip is not large enough to break the ester bonds across the interface, and, hence, subcritical crack growth does not occur. ust above this threshold, the water activity at the crack tip ($p_{\text{H}_2\text{O}}$) is the same as that of the gaseous environment ($p^{\text{eq}}_{\text{H}_2\text{O}}$) and corresponds to a hydrolysis-controlled regime (regime I) where log v is linearly dependent on $\sqrt{G^*}$. Under higher G^*s, $p_{\text{H}_2\text{O}}$ is below $p^{\text{eq}}_{\text{H}_2\text{O}}$ and the $v = v^* \approx$ constant, limited by the transport of water vapor to the bonds ahead of the crack tip (regime II). Regime III occurs when $G \approx G^*_{\text{c}}$ and v reaches dynamic speeds independent of the presence of water (not captured by our model). The behavior of v can be approximated by the following equation [25]:

$$v = \frac{v^*}{1 + (v^*/\Omega)(1/p^{\text{eq}}_{\text{H}_2\text{O}})^n \exp([\Delta H^* - 1/2(\beta\sqrt{G^*})]/RT)}, \tag{1}$$

where ΔH^* is the activation enthalpy for breaking the ester covalent bonds across the interface, R is the universal gas constant, T is the absolute temperature, and v^* is the transport-controlled plateau velocity (regime II) defined as

$$v^* = \frac{cuD_{\text{H}_2\text{O}}p^{\text{eq}}_{\text{H}_2\text{O}}}{n\delta\Sigma} \tag{2}$$

The molar density c of the polymer segments and the water molecules is $\sim 10^3\,\text{mol/m}^3$, and $\text{D}_{\text{H}_2\text{O}}$, the diffusivity of water vapor along the

interface, is $\sim 10^{-12}\,\mathrm{m}^2/\mathrm{s}$ [25]. The parameter n stands for the number of water molecules needed to break one ester bond. Under our experimental conditions, $n = 1$ [25]. The parameter Σ is the areal chain density (number of moles of network strands that must be broken for the crack to advance per unit area of the interface), δ is the transport distance ahead of the crack tip, and u is height of the crack at a distance δ from the crack tip.

The parameter Ω in Equation (1) is a material constant defined as

$$\Omega = \left(\frac{u\zeta}{\Sigma}\right) \exp\left(\frac{\Delta S^*}{R}\right) \tag{3}$$

where ζ is a material constant and ΔS^* is the activation entropy for breaking the ester covalent bonds across the interface.

Equation (1) can be approximated by Equation (4) in regime I and by $v = v^*$ in regime II, respectively [25]:

$$v = (p^{\mathrm{eq}}_{\mathrm{H_2O}})^{\mathrm{n}} \Omega \exp\left[-\frac{\Delta H^* - 1/2(\beta\sqrt{G^*})}{RT}\right] \tag{4}$$

The fit for the unmodified interface was obtained with the following parameters [25]: $\Delta H^* = 81\,\mathrm{KJ/mol}$, $\beta = 18{,}000\,\mathrm{m}\sqrt{\mathrm{J}}$, $\Omega = 8 \times 10^6\,\mathrm{m/s}$, and $n = 1$. The fits for the modified interface were obtained as follows: at the outset, we consider that Σ is the only variable in our model and determine the dependence of v on Σ for both regimes I and II. From Equation (2) it is clear that, in regime II, $v = v^* \propto \Sigma^{-1}$. In Equation (4), for regime I, there are two parameters that are dependent on Σ. The parameter Ω is $\propto \Sigma^{-1}$ [Equation (3)]. In the unmodified case, $V^* \propto \Sigma^{-1}$ and $L \propto \Sigma^{-0.5}$. Hence, the parameter $\beta \propto \Sigma^{-0.75}$.

We next describe the determination of the ratio $f = \Sigma/\Sigma_0$ for the different values of w for which the data on the water-assisted crack growth are shown in Figure 7. Here, Σ_0 stands for the ester areal bond density along the unmodified interface. The ratio f is obtained from the experimentally measured v^* data for the various w using Equation (2). We use the same f ratio to scale the parameter Ω using its inverse dependence on Σ [as shown in Equation (3)]. Now we obtain the parameter β so that a good fit is achieved for our experimental data. Table 3 summarizes the results obtained for f from v^* and β/β_0 obtained from the experiment. Here β_0 represents the parameter β for an unmodified interface. Note that the change in β with the increase in w is much smaller than anticipated from the relation $\beta \propto \Sigma^{-0.75}$ derived for the unmodified interface. The nearly two orders of magnitude increase in f (from v^*) seem reasonable (v^* would decrease because it now requires more water molecules to be

TABLE 3 Comparison of the Ratio of Areal Bond Density Σ/Σ_0 Obtained from v^* (Also Used to Scale the Parameter Ω)

Epoxy interpenetration depth, w (nm)	$f = \Sigma/\Sigma_0$ obtained from v^*	β/β_0 obtained from fit
No modification	1	1
19	15	0.83
25	44	0.73
38	80	0.61

Note: The parameter Σ_0 represents the areal bond density of the unmodified interface. Shown in column 3 are β/β_0 obtained from experimental fit.

transported to the crack tip for the crack front to grow a unit area). The f value calculated from β (using, $\Sigma \propto \beta^{-4/3}$), however, increases by only a factor of two. This increase seems very low for the intermixing that must go on in the interpenetration zone. This also implies that at a given G^* in the regime I, the force experienced by each ester covalent bond across the interface decreases only modestly as the w (and Σ) increase. A possible explanation is that the stress at the crack tip does not simultaneously load all the ester bonds along the interpenetrating interphase.

The parameter β is the only variable that affects the G^*_{th}. Because the dependence of β on Σ is very weak, the increase in G^*_{th} due to interpenetration is not as high as would be predicted if β were $\propto \Sigma^{-0.75}$. Note that we have assumed that the diffusivity of the water vapor is a constant even when w is increased. This is a good assumption because our original model is based on the premise that the water transport occurs along the interface (at a rate that is comparable with the diffusivity of water vapor along the bulk polymers on either side of the interface) and hydrolysis occurs a little distance ahead of the crack tip. Hence, even after the increased interpenetration, the diffusivity of the water vapor along the interphase should remain nearly constant.

CONCLUSION

The interface between an epoxy and a polyimide can be strengthened by converting a thin surface of the polyimide back into its precursor PAA. The epoxy can then be dispensed in solution. The solvent swells the newly created PAA surface layer, thus enabling the interpenetration of the epoxy into the PAA layer. The interface between an unmodified polyimide and the epoxy is very sharp ($\sim$12 nm). The interface between surface-modified polyimide and the epoxy dispensed

without the solvent is also sharp. However, progressive surface modification, followed by dispensing the epoxy in solution, creates an increasingly interpenetrating region of the epoxy and the polyimide leading to a broader interface (interphase). The increase in the fracture energy due to this surface-modification procedure is dramatic. For modest interpenetrations of $\sim 45\,\text{nm}$, the fracture energy is higher than $100\,\text{J/m}^2$ (up from the $25\,\text{J/m}^2$ for the unmodified interface). Further increase in the interpenetration leads to increased fracture energy, until the interface becomes stronger than the individual epoxy beams on either side of the interface.

The surface-modification procedure used also enhances the resistance of the epoxy/polyimide interface to stress-assisted crack growth due to hydrolysis of the ester primary covalent bonds that bridge the interface. The threshold for subcritical crack growth (G^*_{th}) increases and the steady-state subcritical crack-growth velocity (v) for any given energy-release rate $G^* > G^*_{\text{th}}$ decreases. A model for subcritical crack growth that parallels a model developed by Wiederhorn for static fatigue of glass can provide a reasonable fit to our data. The model provides an empirical means to determine the proportional increase in the strand density across the interface. Analysis of the fracture surfaces conducted using SIMS reveals that the crack propagation in the unmodified case occurs along the interface and in the modified case occurs along the newly created epoxy/polyimide interphase layer.

ACKNOWLEDGMENTS

We gratefully acknowledge the support of this research by the Semiconductor Research Corporation (SRC) under Grant No. 635.001. We also appreciate the use of the Ion Beam Analysis Central Facility of the Materials Science Center at Cornell University, which is funded by the NSF-DMR-MRSEC program, and the MRL Central Facilities at UCSB, supported by the NSF under Award No. DMR 0520415. The purchase of a dynamic SIMS at UCSB was funded by an instrumentation grant from NSF Award No. DMR-9703930, and we thank Tom Mates for his assistance in our SIMS measurements. We also acknowledge Inabata Corp., Tokyo, Japan, for providing us the silica fillers used in the filled epoxy.

REFERENCES

[1] Brown, H. R., Yang, A. C. M., Russell, T. P., Volksen, W., and Kramer, E. J., *Polymer* **29**, 1807–1811 (1988).
[2] Lau, J., *Flip Chip Technologies* (McGraw Hill, NY, 1996).

[3] Sarkar, G., Ng, H. W., and Law, S. B., *J. Materials Science Letters* **18**, 423–424 (1999).
[4] Le Gall, C. A., Qu, J., and McDowell, D. L., *Electronics Components and Technology Conference* 430–434 (1996).
[5] Suryanarayana, D., Hsiao, R., Gall, T. P., and McCreary, J. M., *IEEE Transactions on Components, Hybrids, and Manufacturing Technology* **14**, 218–223 (1991).
[6] Gurumurthy, C. K., Norris, L. G., Hui, C. Y., and Kramer, E. J., *The 48th Electronics Components and Technology Conference*, 721–728 (1998).
[7] Gurumurthy, C. K., Jiao, J., Norris, L. G., Hui, C. Y., and Kramer, E. J., *Transactions of the ASME, Journal of Electronic Packaging* **120**, 372–378 (1998).
[8] Hoontrakul, P., Sperling, L. H., and Pearson, R. A., *IEEE Trans. Device Mat. Reliab.* **3**, 159–166 (2003).
[9] Egitto, F. D. and Matienzo, L. J., *IBM Journal of Research and Development* **38**, 423–439 (1994).
[10] Goldblatt, R. D., Ferreiro, L. M., Nunes, S. L., Thomas, R. R., Chou, N. J., Buchwalter, L. P., Heidenreich, J. E., and Chao, T. H., *Journal of Applied Polymer Science* **46**, 2189–2201 (1992).
[11] Vanderlinde, W. E. and Ruoff, A. L., *Journal of Vacuum Science and Technology, B* **6**, 1621–1625 (1988).
[12] Pappas, D. L., Cuomo, J. J., and Sachdev, K. G., *Journal of Vacuum Science and Technology, A* **9**, 2704–2708 (1991).
[13] Satsu, Y., Miura, O., Watanabe, R., and Miyazaki, K., *Transactions of the Institute of Electronics, Information and Communication Engineers C-II* **J74C-II**, 489–497 (1991).
[14] Lee, K. W., Kowalczyk, S. P., and Shaw, J. M., *Macromolecules* **23**, 2097–2100 (1990).
[15] Lee, K. W., Kowalczyk, S. P., and Shaw, J. M., *Langmuir* **7**, 2450–2453 (1991).
[16] Lee, K. W. and Viehbeck, A., *IBM Journal of Research and Development* **38**, 457–474 (1994).
[17] Stoffel, N. C., Hsieh, M., Kramer, E. J., and Volksen, W., *IEEE Transactions on Components, Packaging and Manufacturing Technology B* **19**, 417–422 (1996).
[18] Stoffel, N. C., Zhang, C., and Kramer, E. J., *Application of Fracture Mechanics in Electronic Packaging and Materials: 1995 ASME International Mechanical Engineering Congress and Exposition*, EEP—Vol. 11, MD—Vol. 64, (1995), 79–84.
[19] Stoffel, N. C., Interdiffusion and Adhesion of Polyimides, Ph.D. Thesis, Cornell University (1996).
[20] Kim, S. H., Lee, D. W., Chung, K.-H., Park, J. K., Jaung, J.-Y., and Jeong, S. H., *J. Appl. Polym. Sci.* **86**, 812–820 (2002).
[21] Yun, H. K., Cho, K., Kim, J. K., Park, C. E., Sim, S. M., Oh, S. Y., and Park, J. M., *Polymer* **38**, 827–834 (1997).
[22] Voyutskii, S. S., *Autohesion and Adhesion of High Polymers* (Interscience, New York, 1963).
[23] Wake, W. C., *Adhesion and the Formulation of Adhesives* (Applied Science, London, 1976).
[24] Comyn, J., in *Polymer Permeability*, J. Comyn (Ed.) (Elsevier Applied Science, London, 1985).
[25] Gurumurthy, C. K., Kramer, E. J., and Hui, C.-Y., *International Journal of Fracture* **109**, 1–28 (2001).
[26] Jiao, J., Gurumurthy, C. K., Kramer, E. J., Sha, Y., Hui, C. Y., and Borgesen, P., *Transactions of the ASME, Journal of Electronic Packaging* **120**, 349–353 (1998).

[27] Calistri-Yeh, M., Kramer, E. J., Sharma, R., Zhao, W., Rafailovich, M. H., Sokolov, J., and Brock, J. D., *Langmuir* **12**, 2747–2755 (1996).
[28] Tead, S. F., Kramer, E. J., Russell, T. P., and Volksen, W., *Polymer* **33**, 3382–3387 (1992).
[29] Stoffel, N. C., Hsieh, M., Chandra, S., and Kramer, E. J., *Chemistry of Materials* **8**, 1035–1041 (1996).
[30] Jiao, J., Reaction Kinetics and Morphological Changes at Polymer Interfaces and Surfaces, Ph.D. Thesis, Cornell University (1997).
[31] Sha, Y., Hui, C. Y., Kramer, E. J., Hahn, S. F., and Berglund, C. A., *Macromolecules* **29**, 4728–4736 (1996).
[32] Kanninen, M. F., *International Journal of Fracture* **9**, 83–92 (1973).
[33] Stoffel, N. C., Hsieh, M., Kramer, E. J., and Volksen, W., *IEEE Transactions on Components, Packaging and Manufacturing Technology—Part B* **19**, 417–422 (1996).
[34] Lee, K.-W., *J. Adhes. Sci. Technol.* **8**, 1077–1092 (1994).
[35] Wiederhorn, S. M., *Journal of the American Ceramic Society* **50**, 407–414 (1967).